An early cytoplasmic step of peptidoglycan synthesis is associated to MreB in Bacillus subtilis

Anne-Stéphanie Rueff, Arnaud Chastanet, Julia Dominguez-Escobar, Zhizhong Yao, James Yates, Maria-Victoria Prejean, Olivier Delumeau, Philippe Noirot, Roland Wedlich-Soeldner, Sergio R. Filipe, et al.

Molecular Microbiology (2014) 91(2), 348–362 ■
doi:10.1111/mmi.12467
First published online 13 December 2013

An early cytoplasmic step of peptidoglycan synthesis is associated to MreB in *Bacillus subtilis*

Anne-Stéphanie Rueff,[1,2†] Arnaud Chastanet,[1,2†] Julia Domínguez-Escobar,[3‡] Zhizhong Yao,[1,2‡] James Yates,[4‡] Maria-Victoria Prejean,[1,2] Olivier Delumeau,[1,2] Philippe Noirot,[1,2] Roland Wedlich-Söldner,[3] Sergio R. Filipe[4] and Rut Carballido-López[1,2*]

[1]*INRA, UMR1319 Micalis, F-78352 Jouy-en-Josas, France.*

[2]*AgroParisTech, UMR1319 Micalis, F-78352 Jouy-en-Josas, France.*

[3]*Max Planck Institute of Biochemistry, Am Klopferspitz 18, D-82152 Martinsried, Germany.*

[4]*Laboratory of Bacterial Cell Surfaces and Pathogenesis. Instituto de Tecnologia Química e Biológica, Universidade Nova de Lisboa, 2780-157 Oeiras, Portugal.*

Summary

MreB proteins play a major role during morphogenesis of rod-shaped bacteria by organizing biosynthesis of the peptidoglycan cell wall. However, the mechanisms underlying this process are not well understood. In *Bacillus subtilis*, membrane-associated MreB polymers have been shown to be associated to elongation-specific complexes containing transmembrane morphogenetic factors and extracellular cell wall assembly proteins. We have now found that an early intracellular step of cell wall synthesis is also associated to MreB. We show that the previously uncharacterized protein YkuR (renamed DapI) is required for synthesis of *meso*-diaminopimelate (*m*-DAP), an essential constituent of the peptidoglycan precursor, and that it physically interacts with MreB. Highly inclined laminated optical sheet microscopy revealed that YkuR forms uniformly distributed foci that exhibit fast motion in the cytoplasm, and are not detected in cells lacking MreB. We propose a model in which soluble MreB organizes intracellular steps of peptidoglycan synthesis in the cytoplasm to feed the membrane-associated cell wall synthesizing machineries.

Accepted 18 November, 2013. *For correspondence. E-mail rut.carballido-lopez@jouy.inra.fr; Tel. (+33) 1 34 65 29 55; Fax (+33) 1 34 65 25 21. †These authors contributed equally to this work. ‡These authors contributed equally to this work. The authors have no conflict of interest to declare.

Introduction

Bacterial cell shape is maintained by the stress-bearing cell wall (CW) that envelops the cytoplasmic membrane. In Gram-positive bacteria, the CW is a thick, multilayered structure primarily composed of peptidoglycan (PG) and teichoic acids. The PG meshwork, or sacculus, is a polymer of alternating *N*-acetylglucosamine and *N*-acetylmuramic acid saccharides [poly-(GlcNAc-MurNAc)] cross-linked by short peptides attached to each MurNAc residue. The stem peptides are synthesized as pentapeptide chains that contain both L- and D-amino acid residues and display substantial variability. A di-basic amino acid at the third position allows the formation of peptide cross-bridges between neighbouring glycan chains. In Gram-negative bacteria and Gram-positive bacilli this di-basic amino acid is *meso*-diaminopimelate (*m*-DAP, a lysine precursor present only in bacteria and higher plants), while most other Gram-positive bacteria (including Gram-positive cocci) contain L-lysine at this position.

In *Bacillus subtilis*, the first two steps of the pathway leading to synthesis of *m*-DAP, the so-called DAP pathway, are shared with the biosynthetic pathways for amino acids of the aspartate family (lysine, methionine, threonine and isoleucine) (Fig. 1) (Belitsky, 2002; Rodionov *et al.*, 2003). In these two common steps, L-aspartate is converted to L-aspartate-semialdehyde by enzymes with aspartokinase and aspartate semialdehyde dehydrogenase activities. *B. subtilis* encodes three monofunctional aspartokinase isoenzymes, DapG, LysC and YclM, and a single aspartate semialdehyde dehydrogenase, Asd (Rosner and Paulus, 1971; Chen *et al.*, 1989; 1993; Petricek *et al.*, 1989; Graves and Switzer, 1990; Zhang *et al.*, 1990; Roten *et al.*, 1991; Kobashi *et al.*, 2001). L-aspartate-semialdehyde is then either fed into the methionine/threonine/isoleucine biosynthetic pathways or converted into *m*-DAP via six additional enzymatic steps, for which the corresponding *B. subtilis* genes remain to be characterized (Fig. 1) (Belitsky, 2002). Conversion of L-aspartate-semialdehyde to L-tetrahydrodipicolinate is thought to be catalysed by DapA and DapB (Chen *et al.*, 1993; Belitsky, 2002). Next,

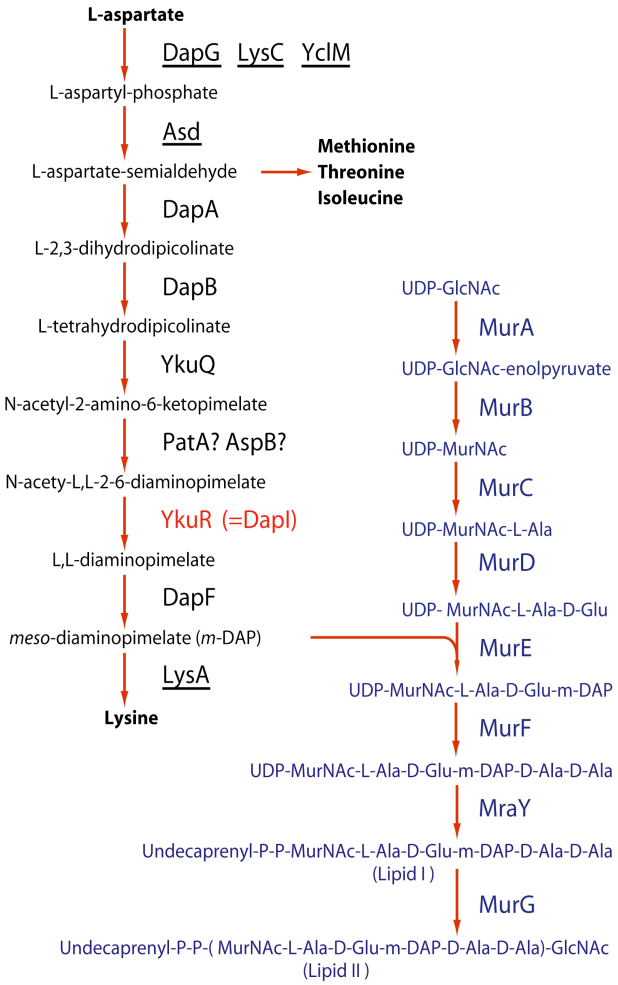

Fig. 1. The DAP/lysine and Mur pathways of *Bacillus subtilis*. The metabolic pathway leading to lysine (in black) interconnects with the Mur biosynthetic pathway of lipid-linked PG intermediates (in blue) via *m*-DAP. In the lysine pathway, underscored proteins were previously characterized in *B. subtilis*. YkuQ and YkuR are sometimes referred to as DapD and DapE respectively due to their similarity with *E. coli* proteins, although their substrates differ (succinylated instead of acetylated derivatives).

certain *Bacillus* species including *B. subtilis* synthesize *m*-DAP from L-tetrahydrodipicolinate in four steps and use acetylated DAP derivatives (DAP acetylase pathway), whereas most eubacteria (including *Escherichia coli*), Archaea and plants utilize the analogous succinylase pathway, where a succinyl residue instead of the acetyl one is used as a blocking group (Weinberger and Gilvarg, 1970; Velasco *et al*., 2002). In *B. subtilis* the first and last step have been suggested to be catalysed by the products of *ykuQ* and *dapF* respectively, based on their similarity with DapD and DapF of other organisms (Chen *et al*., 1993; Belitsky, 2002). The enzymes for the other two steps remain more elusive. The aminotransferase activity carried by DapC in *E. coli* was proposed to be carried by AspB or its paralogue PatA (Belitsky, 2002; Rodionov *et al*., 2003). No orthologue of the *E. coli* DapE protein, which catalyses the deacetylation step in the succinyl-dependent pathway, can be identified by similarity searches, but the missing *B. subtilis N*-acetyl-diaminopimelate deacetylase function was tentatively assigned to YkuR and/or YlmB (Kobashi *et al*., 2001; Belitsky, 2002; Rodionov *et al*., 2003). YlmB was later shown to be involved in the thiamine salvage pathway (and renamed ThiQ) (Jenkins *et al*., 2007). YkuR -the focus of this study- was proposed to be the counterpart of DapE based on the chromosomal location of the *ykuR* gene upstream *ykuQ* (Rodionov *et al*., 2003), but remained uncharacterized. Finally, *m*-DAP is either decarboxylated by LysA to form lysine (Grandgenett and Stahly, 1971) or channelled into the PG precursor biosynthetic (Mur) pathway (Fig. 1).

Like the DAP pathway, biosynthesis of the monomer building block of PG, the PG nucleotide precursor (UDP-MurNAc-pentapeptide), occurs in the cytoplasm, via sequential reactions catalysed by the Mur proteins (Barreteau *et al*., 2008; Lovering *et al*., 2012). Among these, the essential MurE links DAP and PG biosynthetic pathways by catalysing the incorporation of *m*-DAP into the PG precursor to form the tripeptide intermediate UDP-MurNAc-L-Ala-D-Glu-*m*-DAP (Jana *et al*., 2000; Gardete *et al*., 2004) (Fig. 1). Next, the PG nucleotide precursor is transferred onto an undecaprenyl phosphate carrier at the inner leaflet of the cytoplasmic membrane to form the lipid-linked substrate for PG polymerization Lipid II (undecaprenol-PP-MurNAc-pentapeptide-GlcNAc) (Bouhss *et al*., 2008). After translocation across the membrane (Bouhss *et al*., 2008; Mohammadi *et al*., 2011), the disaccharide-pentapeptide units are incorporated into the growing PG sacculus by the action of penicillin-binding proteins (PBPs), which catalyse transglycosylation and transpeptidation reactions (Scheffers and Pinho, 2005; Vollmer and Bertsche, 2008).

PBPs together with PG hydrolases (autolysins) and other morphogenetic determinants are thought to form large multi-enzyme complexes associated with the membrane (Höltje, 1996). Although such complexes have not yet been isolated (Zapun *et al*., 2012), the prevailing model is that they need to be spatially organized by cytoskeletal elements to generate a functional CW architecture (Chastanet and Carballido-López, 2012; Typas *et al*., 2012). In rod-shaped bacteria two separate systems for CW synthesis, each presumably associated with specific PG-synthesizing complexes, coexist: one for cross-wall (septum) formation at the time of division, and one for cylindrical sidewall elongation during growth. Division-specific PG-synthesizing machineries are directed by the tubulin homologue FtsZ while elongation-specific PG-synthesizing complexes are organized by the actin homologue MreB. Accordingly, depletion of MreB or

MreB-associated morphogenetic determinants (MreC, MreD, RodZ or RodA) leads to defects in cylindrical elongation and to cell rounding (Osborn and Rothfield, 2007; Chastanet and Carballido-López, 2012). Over the last decade it was established that MreB proteins form filamentous helical structures along the membrane that position CW elongation complexes (Carballido-López, 2006; Chastanet and Carballido-López, 2012). Consistently, insertion of PG along the sidewalls of *B. subtilis* cells occurs in a banded pattern that depends on the presence of the three MreB isoforms, MreB, Mbl and MreBH (Daniel and Errington, 2003; Tiyanont *et al*., 2006; Kawai *et al*., 2009a). However, using live cell imaging and total internal reflection fluorescence microscopy (TIRFM), we and others recently showed that in growing cells MreB homologues do not form extended helical structures but instead cortical patches that move processively around the sidewalls together with elongation-specific PG-synthesizing factors (Domínguez-Escobar *et al*., 2011; Garner *et al*., 2011; van Teeffelen *et al*., 2011). Furthermore, motility of the complexes was not driven by the polymerization of MreB proteins (i.e. was not treadmilling-based) as expected from an actin-like force-generating mode of action, but powered by PG synthesis itself (Domínguez-Escobar *et al*., 2011; Garner *et al*., 2011). These findings challenged the perceived functional similarity between MreB proteins and eukaryotic actins (Chastanet and Carballido-López, 2012) and raised again the question of the mechanisms underlying MreB morphogenetic function. Our TIRFM results indicated that MreB patches may serve as mechanical clamps that orient and restrict the motility of the extracellular elongation complexes along the membrane (Domínguez-Escobar *et al*., 2011). Two-hybrid and *in vitro* assays revealed interactions between MreB and several Mur enzymes in *Caulobacter crescentus*, *E. coli, Thermotoga maritima* and *Chlamydophila* (Chlamydia) *pneumonia*, indicating that PG precursor synthesis in the cytosol is also associated to MreB (Divakaruni *et al*., 2007; Mohammadi *et al*., 2007; White *et al*., 2010; Gaballah *et al*., 2011; Favini-Stabile *et al*., 2013). These findings have put forward the idea of a large holoenzyme complex associated to MreB filaments in the membrane, which would serve as platforms for both intracellular and extracellular PG biosynthetic machineries. However, the organization of the cytoplasmic steps of PG precursor synthesis and the role of MreB in this process remain to be elucidated.

Here, we show that in *B. subtilis* the YkuR protein (renamed DapI) is essential for synthesis of the PG precursor and that it physically associates with MreB. Subcellular localization studies showed that YkuR is cytosolic. Although the role of the YkuR–MreB interaction remains to be elucidated, our findings are consistent with the existence of MreB-associated steps for PG precursor biosynthesis in the cytoplasm, and suggest that MreB separately co-ordinates intracellular and extracellular PG-synthesizing machineries.

Results

MreB interacts with YkuR in vivo *and* in vitro

To identify novel aspects of MreB function we used a genome-wide yeast two-hybrid (Y2H) screen for interaction partners in *B. subtilis*. We used either full-length (aa 1–337) MreB, or only its N-terminal (aa 1–203) and C-terminal (aa 152–337) domains fused to the C-terminus of the yeast GAL4 DNA-binding domain (BD) as baits to screen three random *B. subtilis* genomic libraries expressing fusions to the GAL4 activation domain (AD). Only positive interactions isolated under highly selective regimes were retained. Two independent rounds of screening per bait followed by rigorous specificity tests (see *Experimental procedures*) yielded four candidate partners of MreB: the squalene synthase YisP, the operon antiterminator SacY, and two proteins of unknown function, YuiC and YkuR. We focus in the present study on the specific interaction found between MreB and YkuR (Fig. 2A). The *ykuR* gene of *B. subtilis* encodes a 374 aa (41 kDa) putative *N*-acetyl-diaminopimelate deacetylase belonging to the peptidase M20 family and presumably involved in the DAP pathway (Roten *et al*., 1991; Rodionov *et al*., 2003). The MreB-interacting fragment of YkuR originally isolated in the screen comprised aa 18–124. This fragment (or full-length YkuR) did not interact with well-expressed BD fusions to MreBH (data not shown). Analysis of a possible interaction with Mbl was not possible as Mbl fusions have not been proven functional so far in two-hybrid assays (data not shown) (Munoz-Espin *et al*., 2009). YkuR is predicted to have a long peptidase domain (aa 65–371) containing a self-interaction domain (aa 170–276) (http://pfam.sanger.ac.uk/). AD and BD fusions to full-length *ykuR* were coexpressed in yeast cells and confirmed the self-interaction *in vivo* (Fig. 2B). Furthermore, gel filtration assays of purified YkuR indicated the presence of YkuR tetramers (Fig. S1A–C). To confirm the specificity of the YkuR–MreB interaction, we purified YkuR-associated protein complexes from *B. subtilis* cell lysates. YkuR was fused to the sequential peptide affinity (SPA) tag, which allows for one- or two-step purification (Zeghouf *et al*., 2004). Unlike cells lacking YkuR (see below), cells containing *ykuR-spa* at the endogenous locus as only copy of *ykuR* in their genome displayed normal growth (Fig. S2A) and morphology (Fig. S2B), indicating that the YkuR–SPA fusion was functional. Western blot analysis of whole-cell extracts showed that levels of endogenously expressed YkuR–SPA progressively increased during exponential phase and decreased again at the onset of stationary phase (Fig. S2A, inset), in agreement with recently pub-

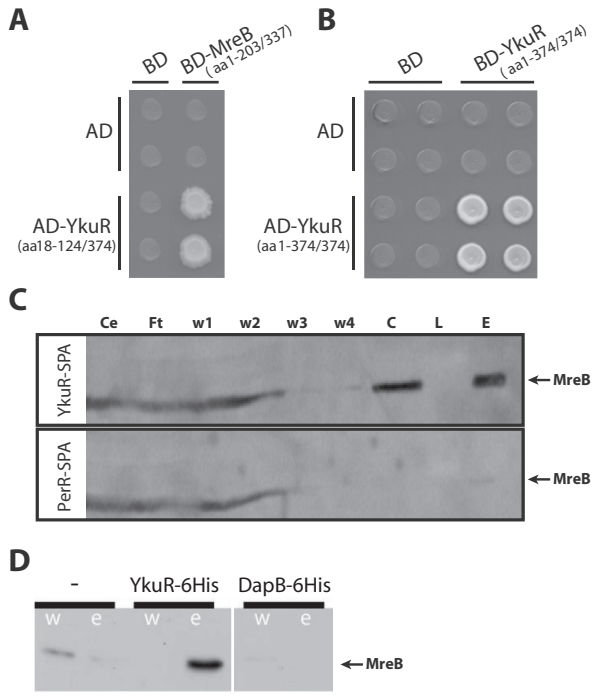

Fig. 2. MreB interacts with YkuR.
A and B. Yeast two-hybrid assay showing the direct interaction of MreB with the YkuR fragment isolated in the screen (A), and self-interaction of full-length YkuR (B). Co-ordinates in amino acid (aa) over the size of the full-length protein. Negative controls included untagged BD (GAL4 DNA-binding domain) and AD (GAL4 activation domain). Pairs of colonies correspond to two independent matings.
C. MreB co-purifies with SPA-tagged YkuR from *B. subtilis* crude extracts. YkuR–SPA and the unrelated PerR-SPA (mock experiment) were purified from whole-cell extracts of strains ASR009 and Bas13 respectively using IgG anti-FLAG resin (see *Experimental procedures* for details). Samples collected during the purification procedure were subject to immunoblot analysis using anti–MreB antibodies. The tracks compare the levels of MreB in the crude extract (Ce), flow-through (Ft), washes (w1 to w4), column-bound material (C) and elution fraction (E). L stands for Ladder.
D. MreB from *B. subtilis* crude extracts is specifically pulled-down by purified YkuR. *B. subtilis* wild-type (strain 168) whole-cell extracts were flushed through Ni-NTA columns either empty (left panel, [–]) or preloaded with affinity-purified recombinant 6His-tagged YkuR ('YkuR-6His') or DapB ('DapB-6His). Samples corresponding to the last wash (w) and the elution fraction by imidazole (e) of each column were subject to SDS-PAGE and immunoblot analysis using anti-MreB antibodies (see *Experimental procedures*).

lished whole-transcriptome data of *B. subtilis* (Nicolas *et al.*, 2012). Cells were grown to mid-exponential phase and collected for SPA-tag analysis. Upon a first purification step, the presence of MreB among the proteins co-eluted with YkuR was tested by Western blot (see *Experimental procedures* for details). A reproducible and specific retention of MreB was detected in the eluate of these pull-down experiments (Fig. 2C). As negative control, a non-related protein of *B. subtilis*, PerR, was SPA-tagged and purified under the same conditions (Fig. 2C). After the second purification step and subsequent liquid chromatography tandem mass spectrometry (MS) analysis, MreB was again specifically detected in the YkuR pull-down complexes (Fig. S2C and D). In contrast, control strains expressing PerR-SPA or other MreB-unrelated SPA fusions (data not shown), or no SPA-tagged protein (Fig. S2D) contained little or no MreB in their eluate. It is important to report that MreB and Mbl are usual contaminants in SPA-tag purifications [systematically 1–2% abundance relative to the purified bait in more than 10 SPA-tag purifications performed in our lab using the method described here (see *Experimental procedures*) (O. Delumeau, unpubl. data)] and thus one should be careful when detecting them in pull-down experiments. However, MreB was co-purified with YkuR–SPA well above the contaminant value [average 10% abundance relative to recovered YkuR ($n = 3$; 10%, 11.1% and 9.4%)], indicating that their interaction is specific. We nevertheless purified recombinant YkuR-6His from *E. coli* and tested it for interaction with MreB from *B. subtilis* cell extracts to further validate our results. Again, MreB was retrieved from the YkuR-containing column, but not from control columns containing no His-tagged protein or recombinant DapB-6His protein (Fig. 2D). Homologues of DapB, the presumed dihydrodipicolinate reductase catalysing the fourth step of the DAP pathway (Fig. 1), have been shown to be homotetramers (Scapin *et al.*, 1995; Cirilli *et al.*, 2003; Janowski *et al.*, 2010; Girish *et al.*, 2011). Like YkuR-6His, DapB-6His was soluble and properly folded (forming tetramers) as shown by gel filtration (Fig. S1B and D).

Taken together, these experiments indicate that YkuR and MreB associate *in vitro* and directly bind to each other *in vivo*.

YkuR is essential for growth and cell morphogenesis

The interaction of MreB with a protein presumably involved in PG precursor biosynthesis prompted us to analyse the phenotype of *ykuR* mutant cells in detail. *YkuR* was reported to be essential in a systematic inactivation study of *B. subtilis* genes (Kobayashi *et al.*, 2003). Consistent with this, we were unable to construct a null *ykuR* mutant by direct replacement of the gene with an antibiotic resistance cassette. Instead, we constructed a conditional mutant in which the endogenous copy of *ykuR* was placed under control of the isopropyl β-D-1-thiogalactopyranoside (IPTG)-inducible promoter P_{spac} (Vagner *et al.*, 1998). Growth of the YkuR depletion strain was IPTG-dependent and highly sensitive to the IPTG concentration in both LB and minimal medium (Fig. S3A and B respectively), confirming that YkuR is indeed essential for growth. At IPTG concentrations ≥ 0.5 mM *ykuR* mutant cells grew at rates comparable to wild-type (Fig. 3A, Figs S3 and S4A). Thus,

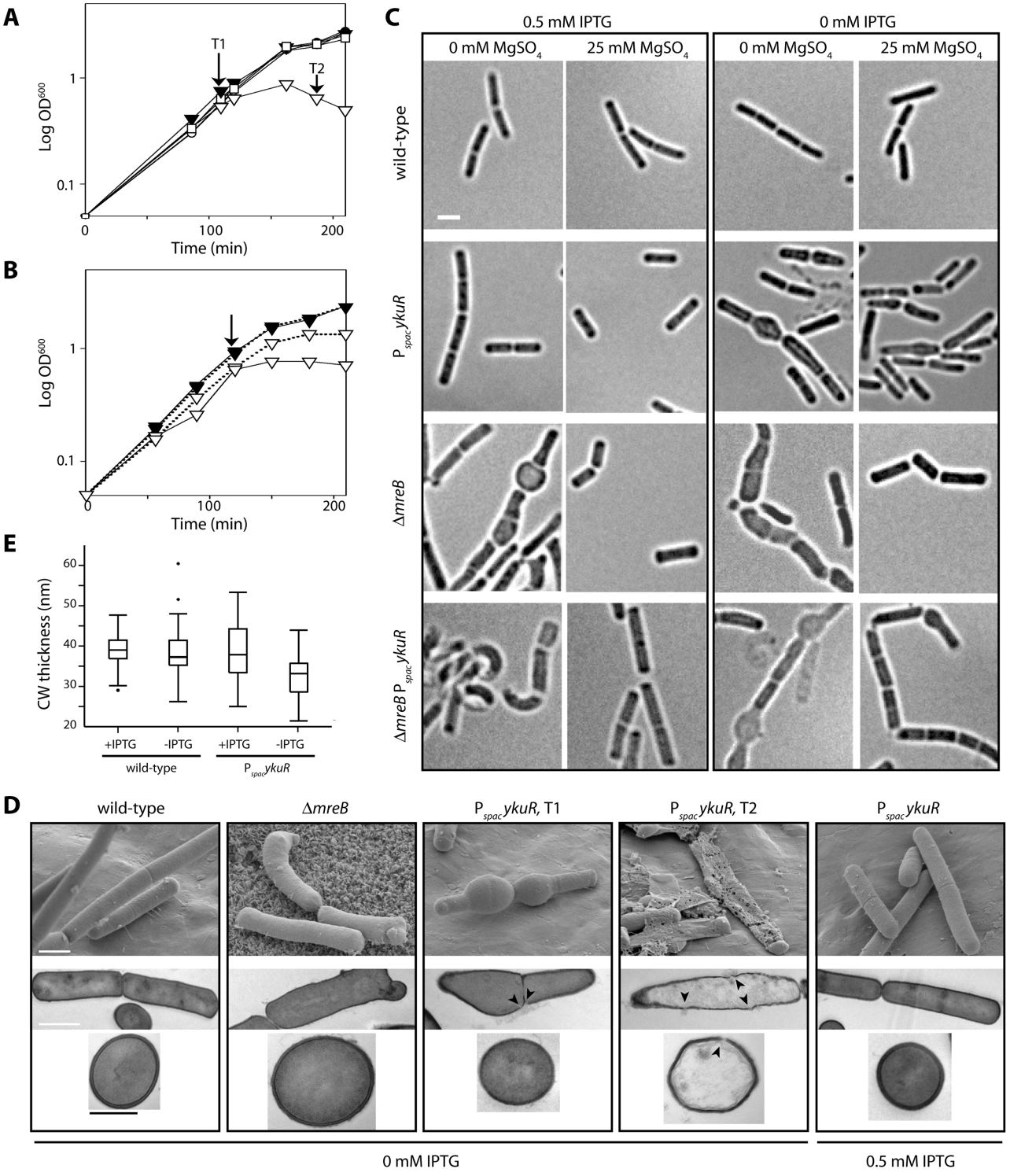

0.5 mM IPTG was considered the optimal inducer concentration and used thereafter in our experiments.

We next analysed the effects of YkuR depletion in detail. In the presence of IPTG, cells showed no obvious morphological defects (Fig. 3C). When IPTG was removed, *ykuR* mutant cells were quickly affected. After approximately three to four generations, cultures stopped growing and lysed (Fig. 3A and Fig. S4A). Cell shape was also severely affected: most cells began to swell and round up before eventually lysing. This phenotype is reminiscent of that displayed by Δ*mreB* cells under comparable conditions (Formstone and Errington, 2005) (Fig. 3C). It also resem-

Fig. 3. YkuR is essential for growth and cell shape maintenance.
A. Growth curves of the wild-type reference strain (ASR053, circles), the YkuR-depletion strain (P_{spac}*ykuR*, ASR032; triangles) and the Δ*mreB* strain (3725, squares). Cells were grown at 37°C in LBT medium with kanamycin and 0.5 mM (black symbols) or without (open symbols) IPTG. Samples of the cells shown in (D) were taken for microscopy at the times indicated by 'T1' and 'T2'.
B. Growth curves of the YkuR-depletion strain (P_{spac}*ykuR*, ASR032) grown at 37°C in LBT medium with kanamycin and 0.5 mM (black triangles) or without (open triangles) IPTG, and in the absence (full lines) or presence (dotted lines) of 25 mM $MgSO_4$. Samples of the cells shown in (C) were taken for microscopy at the time indicated by an arrow.
C. Effect of IPTG and Mg^{2+} on the morphology of cells of the wild-type (ASR053), the YkuR-depletion (P_{spac}*ykuR*, ASR032), the Δ*mreB* (3725) and the Δ*mreB* P_{spac}*ykuR* (ASR001) strains. Cells were collected at the time indicated with an arrow in (B). Scale bar: 2 μm.
D. Electron micrographs of cells of the same strains grown in the presence or in the absence of IPTG as indicated. Samples were taken at the times 'T1' and 'T2' indicated with arrows in (A) and imaged by scanning electron microscopy (upper panels) and transmission electron microscopy (middle panels, selection of longitudinal sections; lower panels, transversal sections). Arrowheads indicate holes in the cell wall. White scale bar: 1 μm; black scale bar: 0.5 μm.
E. Boxplots of cell wall thickness of cells collected at 'T1' in (A).

bles the effects seen upon repression of the *murE* operon (Daniel and Errington, 2003), which encodes the essential UDP-MurNAc tripeptide synthetase MurE (Michaud *et al*., 1990), responsible for incorporating *m*-DAP into the PG precursor (Fig. 1). Control experiments showed that the defects observed upon YkuR depletion were not due to polar effects on the downstream *ykuS* gene, which codes for a non-essential small protein of unknown function (Fig. S4). In *B. subtilis*, the viability and/or cell shape defects of *mreB* and several CW mutants can be rescued by addition of high levels of magnesium (Mg^{2+}) (Chastanet and Carballido-López, 2012). In contrast to Δ*mreB* cells, addition of 25 mM Mg^{2+} did not rescue the lethality (Fig. S3A) and morphology defects (Fig. 3C) of *ykuR* mutant cells. It nevertheless ameliorated their growth at low IPTG concentrations (Fig. S3A) and upon IPTG removal (Fig. 3C), and delayed the appearance of morphological defects and the eventual lysis of YkuR-depleted cells (Fig. 3B). Finally, a double *mreB ykuR* mutation was also lethal (data not shown). Upon depletion of YkuR, Δ*mreB* cells lysed and were also not rescued by Mg^{2+} (Fig. 3C), indicating that *ykuR* is epistatic.

In summary, the phenotypic consequences of YkuR-loss were consistent with a defect in PG synthesis, and thus in agreement with its predicted role in the DAP/lysine pathway. Importantly, they were not resulting from inhibition of protein synthesis due to starvation of L-lysine, which is directly produced from *m*-DAP by LysA (see Fig. 1). LysA is essential in minimum medium but not rich LB medium (our experimental conditions), where *lysA* mutant cells grow like wild-type cells (Kobayashi *et al*., 2003; Brans *et al*., 2004). Consistently, addition of up to 1 mg ml^{-1} lysine did not restore viability of YkuR-depleted cells in either LB (Fig. S3C) or minimal medium (Fig. S3D), while 50 μg ml^{-1} of lysine restores the auxotrophy of *lysA* mutant cells in minimal medium (Brans *et al*., 2004).

Integrity and synthesis of the cell wall are affected in ykuR *mutant cells*

We next examined the morphological defects induced by the loss of YkuR by scanning and transmission electron microscopy (SEM and TEM). At early time points after YkuR-depletion, before lysis occurred (T1 in Fig. 3A) we observed widening of cells at or near new division sites (Fig. 3D, P_{spac}*ykuR*, T1; and Fig. S5A and B), similar to *mreB* mutant cells (Formstone and Errington, 2005). In addition, depletion of YkuR resulted in thinner sidewalls [Fig. 3E, control wild-type strain: 38.5 ± 5.1 nm (n = 130), YkuR depletion: 32.2 ± 5.2 nm (n = 151), $P < 0.001$], and some cells displayed holes along their sidewalls through which their cytoplasmic contents leaked (arrowheads in Fig. 3D). Many empty sacculi with multiple holes could be observed after prolonged depletion, when cultures started lysing (T2 in Fig. 3A and D, Fig. S5A). Taken together, these observations suggested a reduction of CW integrity in cells lacking YkuR, likely due to inhibition of CW synthesis. To directly monitor CW synthesis in the absence of YkuR, we stained cells with fluorescently labelled vancomycin (Van-FL), which is incorporated at sites of nascent PG insertion (Daniel and Errington, 2003; Tiyanont *et al*., 2006). As shown in Fig. 4A, in the presence of inducer we observed staining patterns similar to wild-type cells, with the typical banded pattern along the cylinder, intense staining at ongoing or recent division sites and no label at mature cell poles (Daniel and Errington, 2003; Tiyanont *et al*., 2006; Kawai *et al*., 2009a). In the absence of inducer, YkuR-depleted cells exhibited progressive reduction of Van-FL staining along the sidewalls, while staining at division sites was enhanced. This Van-FL pattern was again very similar to that displayed by *mreB* mutants (Kawai *et al*., 2009a) and by cells lacking *murE* (Daniel and Errington, 2003). We concluded that PG synthesis is severely compromised in cells lacking YkuR.

Using TIRFM, we recently showed that the motility of MreB patches is powered by PG synthesis. A reduction of the available PG precursor pool led to a reduced velocity of the movement of patches, while inhibition of PG synthesis completely blocked movement (Domínguez-Escobar *et al*., 2011; Garner *et al*., 2011). To confirm that PG synthesis was blocked in the absence of YkuR, presumably by inhibition of PG precursor synthesis, we analysed motility of GFP–MreB patches in YkuR-depleted cells by

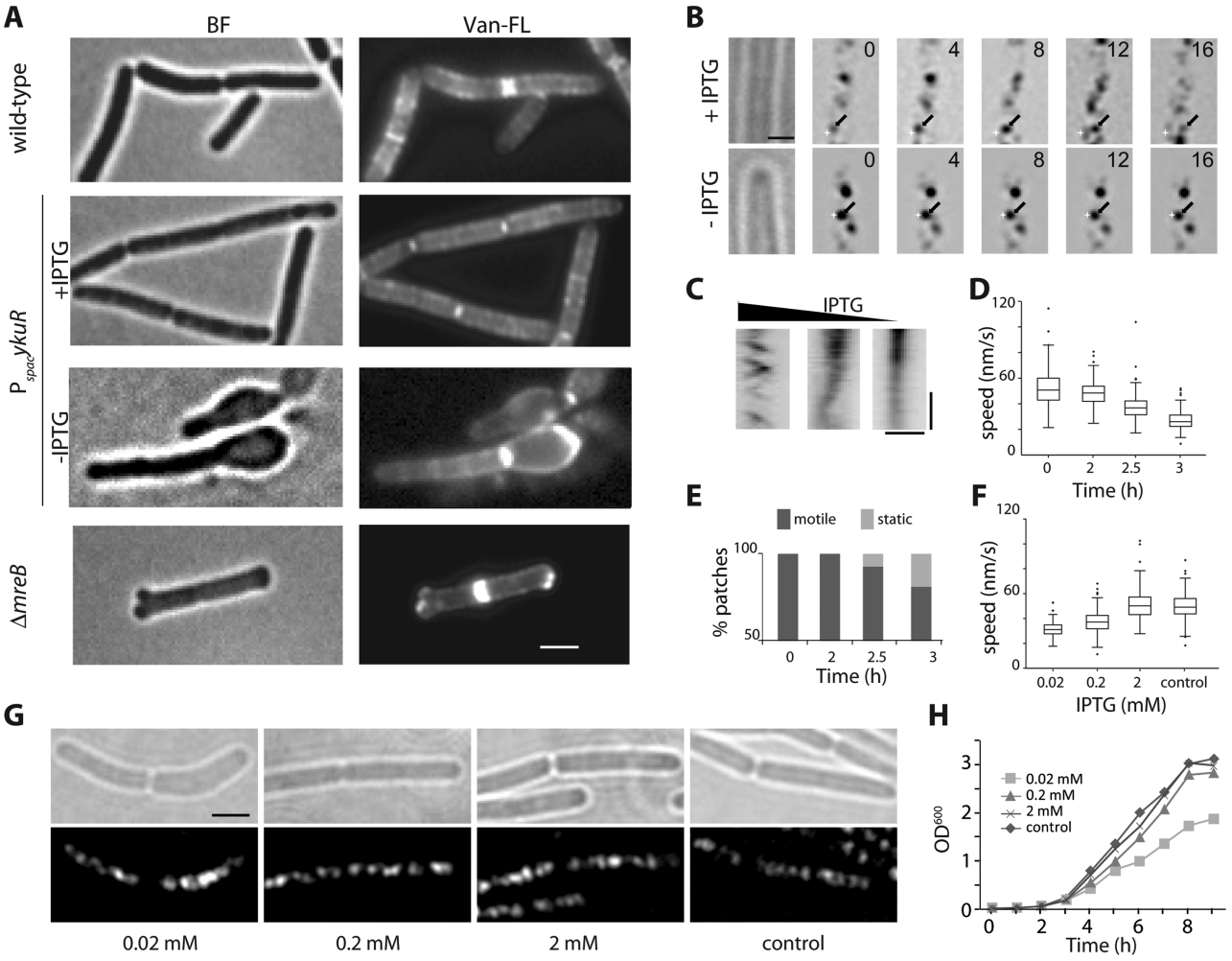

Fig. 4. Cell wall synthesis is inhibited in YkuR-depleted cells.
A. Vancomycin staining (Van-FL) of wild-type (ASR053), P_{spac}*ykuR* (ASR032, in the presence '+ITPG' or absence '–IPTG' of 0.5 mM IPTG) and Δ*mreB* (3725) cells grown exponentially in LBT medium. BF, corresponding bright-field images. Scale bar: 2 μm.
B–H. Effect of YkuR depletion on the dynamics of MreB patches. Cells (strain RWSB357) were grown at 30°C in the presence of 0.5% xylose (to allow *gfp-mreB* expression), and with (0.5 mM unless indicated otherwise) or without IPTG (to allow or not expression of *ykuR*) and imaged by time-lapse TIRFM. (B) MreB patches movement across the cell (arrows). White crosses mark the initial position of the patches tracked. Numbers indicate time in seconds. The corresponding bright-field images are shown on the left. Scale bar: 1 μm. (C) Typical kymographs of MreB patches during depletion of YkuR (IPTG gradient) showing normal motility (left), partial arrest (middle) and complete arrest (right). Vertical time bar: 30 s; horizontal scale bar: 1 μm. (D) MreB patch speed boxplots before (0) and upon washout of IPTG. (E) Per cent of motile versus static MreB patches in *ykuR* cells before (0, $n = 180$) and 2 h ($n = 171$), 2.5 h ($n = 326$) and 3 h ($n = 189$) after removal of IPTG. (F–H) Effect of YkuR levels on speed (F) and distribution (G) of MreB patches, and on cell growth (H). RWSB357 was grown in the presence of 0.02, 0.2 and 2 mM IPTG. Strain RWSB1 was used as control for GFP–MreB patches motility. Corresponding bright-field images are shown in the top panels in (G). Scale bar: 1 μm.

TIRFM. As predicted, depletion of YkuR led to a reduction of the motility of MreB patches, with patch speed gradually slowing down and patches eventually coming to a complete halt (Fig. 4B–E). In addition, and to exclude an indirect effect on patch motility in YkuR-depleted dying cells, we also found reduced patch speed at steady state when *ykuR* conditional cells were grown in the presence of low concentrations of IPTG (Fig. 4F). In the presence of 0.2 mM IPTG patch speed was significantly lower, although no effects on cell shape (Fig. 4G) or growth rate (Fig. 4H) were yet observed. When the levels of inducer were further dropped down to 0.02 mM IPTG, motility of MreB patches was further reduced, growth rate was also significantly reduced and cells displayed clear morphological defects (Fig. 4F–H). No effect was seen on the distribution and/or the density of MreB patches at any of the tested IPTG concentrations (Fig. 4G).

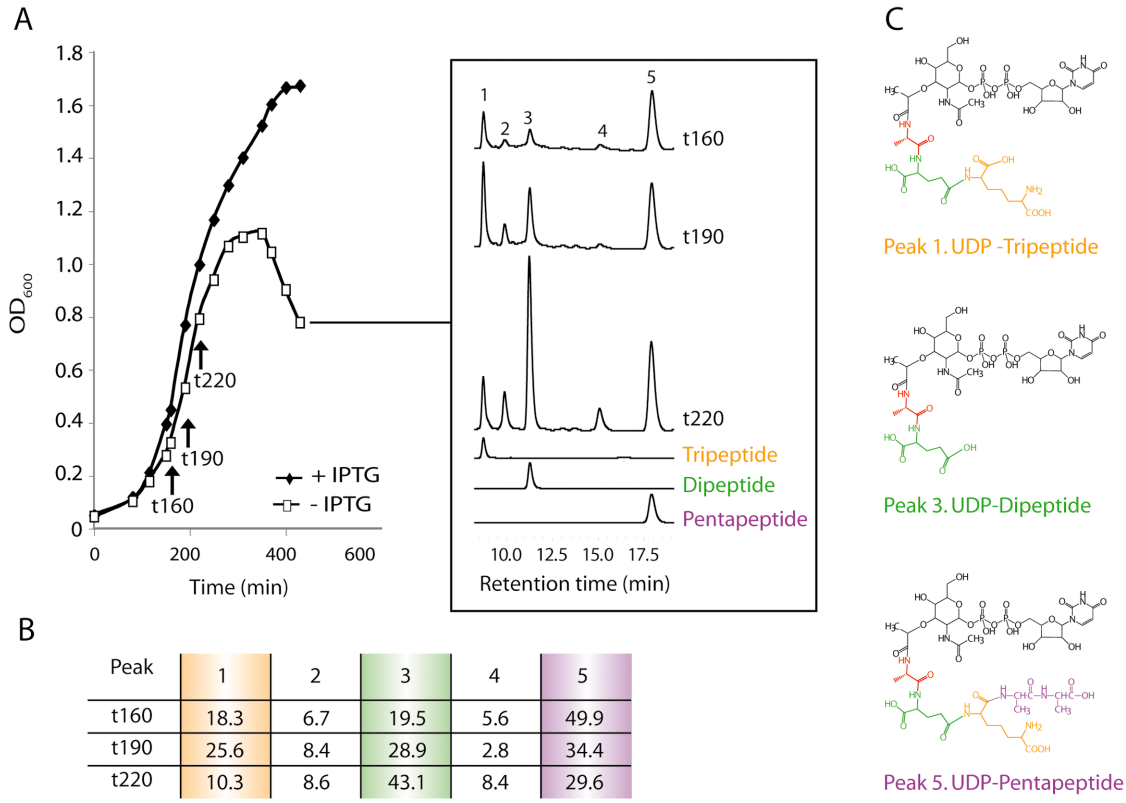

B

Peak	1	2	3	4	5
t160	18.3	6.7	19.5	5.6	49.9
t190	25.6	8.4	28.9	2.8	34.4
t220	10.3	8.6	43.1	8.4	29.6

Fig. 5. UDP-dipeptide peptidoglycan precursors accumulate in the cytoplasm of YkuR-depleted cells.
A. HPLC analysis of the cytoplasmic PG precursor pool during depletion of YkuR. Strain ASR032 (P_{spac}*ykuR*) was grown at 37°C in LB medium in the presence and in the absence of IPTG (left; growth curve). Samples were collected at the indicated time points (in minutes, relative to the IPTG washing-out) and analysed by HPLC (right; corresponding HPLC profiles). Purified tripeptide, dipeptide and pentapeptide precursors were run as controls.
B. Integration of peaks 1 to 5 present in the HPLC runs of strain ASR032 shown in (A). The areas are shown as percentage of the total area of the peaks in the profile.
C. Structure of the molecules identified by MS analysis of purified peaks 1, 3 and 5. Each peptidyl residue is coloured differently: L-Ala, red; D-Glu, green; *m*-DAP, orange; D-Ala, purple.

In summary, our results show that depletion of *ykuR* leads to inhibition of sidewall synthesis presumably from a block in PG precursor synthesis.

YkuR is essential for synthesis of cytoplasmic peptidoglycan precursors

Comparative analysis of genes of the lysine biosynthetic pathway suggested that *B. subtilis* YkuR may catalyse the formation of L,L-diaminopimelate (Rodionov *et al.*, 2003). If this was the case, synthesis of *m*-DAP and thus its addition to the dipeptide cytoplasmic precursor (UDP-MurNAc-L-Ala-D-Glu) by the action of MurE, to form the tripeptide cytoplasmic precursor (UDP-MurNAc-L-Ala-D-Glu-*m*-DAP) (Fig. 1) (Jana *et al.*, 2000; Gardete *et al.*, 2004), would be prevented in the absence of YkuR, leading to accumulation of UDP-MurNAc-dipeptide. To test this, we analysed the composition of the cytoplasmic PG precursor pool during depletion of YkuR, before the onset of cell lysis so as to minimize the loss of soluble metabolites, by high pressure liquid chromatography (HPLC) coupled to MS analysis. Soon after depletion, the HPLC profile of *ykuR* cells showed several peaks (labelled 1 to 5, Fig. 5 and Fig. S6) that were not detected in cells containing YkuR (Fig. S6). This was probably due to accumulation of PG precursors upon disruption of PG synthesis, and might take place well before any growth defect or morphological change was detected in *ykuR* mutant cells. Notably, as YkuR depletion progressed, peak 3 importantly accumulated while peaks 1 and 5 slightly decreased (Fig. 5A and B). As expected, the molecular weight (MW) of the PG precursor eluted in peak 3 corresponded to the mass calculated for the UDP-dipeptide precursor (Fig. 5C, MW peak 3: 879.2 Da, UDP-MurNAc-Ala-Glu). The mass of peaks 1 and 5 corresponded to those of the UDP-tripeptide and UDP-pentapeptide precursors respectively (Fig. 5C, MW peak 1: 1051.3 Da, UDP-MurNAc-Ala-Glu-*m*-DAP; MW peak 5: 1193.3 Da, UDP-MurNAc-Ala-Glu-*m*-DAP-

Ala-Ala). Furthermore, these two peaks had the same retention time as the peaks that accumulated when wild-type cells were incubated with D-cycloserine and vancomycin (Fig. S6A). These antibiotics inhibit different steps of PG synthesis and lead to the accumulation of tripeptide and pentapeptide PG precursors respectively (Kohlrausch and Höltje, 1991). The composition of the purified PG precursors was validated by analysing the spectra obtained by matrix-assisted laser desorption/ionization (MALDI-TOF/TOF) MS. No abnormal incorporation of lysine, which is present at the place of *m*-DAP in most Gram-positive bacteria, occurred in YkuR-depleted cells, as shown also by comparison to the control profile of *Staphylococcus aureus* cells treated with vancomycin, i.e. accumulating UDP-tripeptide precursor with lysine at the third position (Fig. S6A). In contrast to the *ykuR* mutant, the PG precursor pool of the *mreB* mutant showed no significant differences relative to the wild-type strain (Fig. S6B).

Finally, complementary analysis of the muropeptide composition of the sacculus of YkuR-depleted cells showed abnormal accumulation of disaccharide dipeptide (monomeric muropeptide) and concomitant reduction in dimeric muropeptide (Supplemental Experimental Procedures; Supplemental Data and Fig. S7). This was also in full agreement with a blockage in *m*-DAP synthesis and with the accumulation of dipeptide precursors in the cytoplasm of YkuR-depleted cells (Fig. 5). Incorporation of such PG precursor form, lacking *m*-DAP (and thus the di-basic amino acid mediating transpeptidation), is expected to result in a reduced degree of cross-linking of the sacculus, reflected by the reduction of transpeptidated subunits (dimeric muropeptides) observed in *ykuR* cells. Consistently, *ykuR* mutants displayed increased sensitivity to lysozyme (data not shown) and a thinner, weakened sacculus prone to lysis (Fig. 3).

YkuR forms MreB-dependent diffusive foci in the cytoplasm

To gain insight into the YkuR–MreB interaction in *B. subtilis* cells, we analysed the localization of a GFP–YkuR fusion. Cells expressing *gfp-ykuR* as the only copy of *ykuR* in the genome displayed no growth or morphology defects (data not shown), indicating that the fusion was fully functional. When imaged by conventional epifluorescence microscopy, GFP–YkuR displayed an essentially uniform signal in the cytoplasm (Fig. S8A). Western blot analysis using anti-GFP antibodies showed that the expected GFP–YkuR fusion protein was correctly produced (Fig. S8B) and that cytoplasmic localization was not a result of protein degradation. Consistently, a C-terminal GFP fusion exhibited comparable diffuse localization (data not shown). Localization of a subpopulation of YkuR at the membrane, where it could interact with MreB patches, could be masked by the abundant cytosolic signal. We therefore imaged cells by TIRFM, which allows detection of cortical signals with much higher contrast (Domínguez-Escobar *et al*., 2011; Spira *et al*., 2012). Under true TIRF illumination (total internal reflection) no membrane-associated signal could be observed under a range of imaging and growth conditions. GFP–YkuR fluorescence was very weak and largely diffuse, consistent with underlying cytosolic localization (Fig. S8A). Interestingly, weak foci-like signals were sometimes observed over the uniform fluorescence background, moving randomly through the field of view also consistent with cytosolic diffusion (data not shown). To determine if these were discrete entities bumping into the membrane or random fluctuations of freely diffusing fluorescence signal, we used highly inclined laminated optical sheet (HILO, also referred to as 'quasi-' or 'pseudo-TIRF') microscopy, a technique that takes a middle ground between TIRFM and epi-illumination (Tokunaga *et al*., 2008). Slightly varying the laser light incident angle from total internal reflection to a subcritical angle increased GFP–YkuR signal intensity in a volume close to the membrane while reducing the high background scatter responsible for the poor contrast of epi-illumination. Under HILO illumination, we observed foci uniformly distributed in the cytoplasm in virtually all cells (94%, $n = 105$) expressing GFP–YkuR (Fig. 6). YkuR foci were ~ 250 nm (4–5 pixels; 1 pixel = 0.06 μm), indicating that they were diffraction-limited (Fig. S9A and B). Similar foci were not observed in control cells expressing soluble GFP, which displayed a homogeneous fluorescence signal (Fig. 6 and Fig. S9B–C). Time-series using continuous irradiation and rapid detection indicated that GFP–YkuR foci exhibited rapid, likely diffusive, movement in the cytoplasm (Movie S1, left panel). Strikingly, in the absence of *mreB*, GFP–YkuR

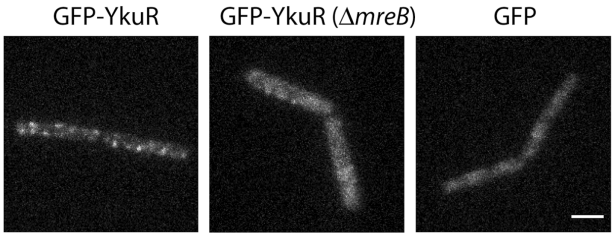

Fig. 6. GFP–YkuR forms cytoplasmic foci in the presence of MreB. HILO microscopy fluorescence images of cells expressing GFP–YkuR in the presence (strain ASR026) and in the absence (ASR166) of MreB growing exponentially at 37°C in LBT medium with 0.2% xylose. In the absence of MreB, cell width increased and YkuR diffraction-limited foci were no longer detected. Cells expressing soluble GFP (ASR111) grown in the same conditions were used as control. In HILO imaging the laser beam penetrates the sample obliquely, increasing the fluorescence signal and illuminating deeper into the cell relative to TIRF (but still shallower relative to epi-illumination) while keeping a low background and a very good signal-to-noise ratio. Exposure time, 10 ms. Scale bar represents 2 μm.

signal resembled that of free-diffusing cytoplasmic GFP in most cells (79%, $n = 115$; Fig. 6 and Movie S1), indicating that YkuR foci are MreB-dependent.

Discussion

Studying enzymes of the Mur and DAP/lysine biosynthetic pathways is of special interest as most of these enzymes are essential in eubacteria but have no homologues in mammalian cells, which makes them great antibiotic targets (Hutton *et al*., 2003; Lovering *et al*., 2012). No *bona fide* homologue to DapE, which deacetylates *N*-succinyl-DAP to produce L,L-DAP in the succinyl-dependent pathway of *E. coli*, exists in *B. subtilis*. However, Rodionov *et al*. postulated that YkuR could catalyse the deacetylation step based on the presence of the *ykuR* gene directly downstream *ykuQ* (homologous to *E. coli dapD*) in bacilli, and as part of a long lysine biosynthetic operon in several organisms (Rodionov *et al*., 2003). We have provided further support for this functional prediction by showing that in *B. subtilis* CW synthesis is inhibited and dipeptide PG precursor subunits accumulate in the absence of YkuR. Because *B. subtilis* uses the acetyl- and not the succinyl-dependent pathway to produce *m*-DAP, we propose to rename this protein DapI (instead of DapE as its *E. coli* counterpart). Two additional relevant conclusions could be drawn from our analysis of the muropeptide composition of the *dapI (ykuR)* mutant. First, the accumulation of disaccharide dipeptide in the sacculus of *dapI* cells (in addition to the accumulation of UDP-dipeptide precursor in their cytoplasm) indicated that this abnormal PG precursor can be formed, exported and incorporated into the CW through transglycosylation at the place of disaccharide pentapeptide (the substrate for PG polymerization). Accumulation of dipeptide and tripeptide forms has been observed in the sacculus of *S. aureus* (Ornelas-Soares *et al*., 1994; Gardete *et al*., 2004; Sobral *et al*., 2006) but was not previously reported for *B. subtilis*. Second, *m*-DAP residues were not replaced by abnormal variants of *m*-DAP or by lysine (available in the growth medium) as alternative substrate for transpeptidation in DapI-depleted cells. In *E. coli* and other bacteria, analogues of *m*-DAP including DAP stereoisomers can be accepted as MurE substrates (Ito and Strominger, 1973; Mengin-Lecreulx *et al*., 1988; 1994; Richaud *et al*., 1993; Auger *et al*., 1996), while different isoenzymes of MurE, one that adds L-Lys and one that adds *m*-DAP, exist in *Bacillus sphaericus* (Anwar and Vlaovic, 1986). Our results show that MurE is highly specific for *m*-DAP in *B. subtilis*. These observations are important in their own right because they provide valuable insights into the structure of the *B. subtilis* CW.

DapI-depleted cells displayed morphological defects before eventually lysing similar to MreB-depleted cells (Formstone and Errington, 2005). However, in contrast to *mreB* mutant cells, high levels of Mg^{2+} did not rescue the lethality of *dapI* (or *dapI mreB*) mutants, nor the cell shape defects and lysis of DapI-depleted cells, as expected if DapI is responsible for an essential step of the synthesis of the PG building blocks. High Mg^{2+} did nevertheless ameliorate the phenotype of cells growing with limiting amounts of DapI, which have thinner CW with a reduced degree of cross-linking. This is consistent with the idea that Mg^{2+} has an indirect structural stabilizing role, and rescues mutants affected in different aspects of shape determination and PG synthesis by stiffening their cell envelope, counteracting deleterious effects of weakened PG sacculi. Empirical evidence to support this hypothesis or to pinpoint the structural feature involved in the rescue effect of Mg^{2+} will provide important insights into the molecular organization of the CW.

Using several biochemical approaches and Y2H assays, we showed that DapI (YkuR) interacts with MreB. Interestingly, YkuQ, which was also proposed to belong to the DAP pathway (Fig. 1), was also pulled down in MreB complexes in a recent report (Kawai *et al*., 2011). *ykuQ*, the orthologue of the *E. coli dapD* gene, lies directly upstream *dapI*. Analysis of their expression profile in last-generation whole-transcriptome data (Nicolas *et al*., 2012) shows that *ykuQ* is co-transcribed with, and the most positively correlated gene to (Pearson correlation coefficient, 0.94), *dapI*. Noteworthy, Mbl and the PG precursor synthetic enzymes MurA and MurB were also found with significant protein abundance index [*pai*, established according to Ishihama *et al*., (2005)] in our DapI complexes (Fig. S2D), and MurF was pulled down in MreB complexes (Kawai *et al*., 2011). These findings indicate that an intricate network of interactions between MreB proteins and enzymes of the DAP and Mur pathways exists in *B. subtilis*. Co-pelleting and two-hybrid assays also revealed interactions of Mur enzymes with MreB in the Gram-negative *C. crescentus* (Divakaruni *et al*., 2007; White *et al*., 2010), *E. coli* (Mohammadi *et al*., 2007) and Chlamydia (Gaballah *et al*., 2011). More recently, *in vitro* interactions were detected between recombinant MreB and MurD, MurE, MurF and MurG of *T. maritima* (Favini-Stabile *et al*., 2013). It is currently unknown where these Mur–MreB interactions take place in the cell and what their exact role is, but these findings put forward a model in which MreB organizes multi-enzyme complexes involved in PG precursor synthesis in the cytoplasm. Our findings reinforce this model and expand it to Gram-positive bacteria. Furthermore, we show that not only Mur enzymes but also those of the branching DAP pathway are in MreB-associated complexes. Bringing together Mur and DAP enzymes would result in reaction coupling and thus metabolic channelling of the PG precursor intermediates. Consistently, we found that like DapI, MurE, which links the DAP and Mur biosynthetic pathways, specifically interacted with MreB in pull-down experiments

(Fig. S10A) and formed diffusive diffraction-limited foci in the cytoplasm under HILO illumination (Fig. S10B and Movie S2).

What is the specific role of the MreB–DapI interaction? Where does it take place? HILO's dramatic increase in signal-to-background over epi-illumination showed that DapI and MurE form diffusing foci in the cytoplasm, and TIRFM analysis found no evidence to suggest that a subpopulation of DapI or MurE interacts with MreB polymers in the membrane. These are not the first examples of proteins found to interact but not to colocalize with MreB patches. PBP1, PBP2b, PBP2c, PBP3, PBP4, PbpI and LytE physically interact with MreB proteins (Carballido-López *et al.*, 2006; Kawai *et al.*, 2009b; 2011) but were also not detected moving together with MreB patches. Instead, they formed foci that rapidly diffused on the cell surface (Domínguez-Escobar *et al.*, 2011). The interaction between MreB and some of these enzymes may be transient and not resolvable on the microscopic timescale. Alternatively, very few molecules may interact (and move along) with MreB patches. These might only (and hardly) be detected using single-molecule approaches. Our finding that DapI forms foci in the cytoplasm that were not detected in the absence of MreB suggested an alternative scenario, where DapI interacts with soluble MreB in the cytoplasm (Fig. 7). It has been shown that there is an important subpopulation of free, unpolymerized MreB [referred to as globular MreB (gMreB) by analogy to G-actin] displaying fast motion characteristic of Brownian diffusion in the cytoplasm (Kim *et al.*, 2006). Actin monomer-binding proteins are abundant and contribute to various actin-dependent cellular processes in eukaryotic cells. Although completely disregarded to date, MreB monomer-binding proteins may exist in bacterial cells too. Interestingly, the diffusion coefficient displayed by the unpolymerized MreB form was significantly slower than expected for a free cytoplasmic protein of similar size (Kim *et al.*, 2006). Such slower diffusion indicated that the movement of soluble MreB is restricted by a yet uncharacterized force, and raised the possibility that unpolymerized MreB interacts either with the cell membrane or with a larger protein complex in the cytoplasm (Kim *et al.*, 2006). Notably, DapI foci were still detected using up to 30 ms exposure time in our HILO time-lapses (Fig. S9C). During this exposure time, assuming that $\langle x^2 \rangle = \langle [x(t + \Delta t) - x(t)]^2 \rangle = 4Dt$ for two-dimensional diffusion [where $\langle x^2 \rangle$ is the mean-squared displacement during the time Δt for a molecule of diffusion coefficient D (Dehmelt and Bastiaens, 2010)], GFP freely diffusing in the bacterial cytoplasm [$D = 7.7\ \mu m^2\ s^{-1}$ first found by fluorescence recovery after photobleaching (FRAP) and photoactivation (PA) (Elowitz *et al.*, 1999) and $\sim 13\ \mu m^2\ s^{-1}$ found more recently by single molecule tracking (English *et al.*, 2011)] would move on average ~ 1–1.3 μm, making such foci irresolvable. Diffusion coefficient decreases however with increasing molecular size (Elowitz *et al.*, 1999; Kumar *et al.*, 2010; Nenninger *et al.*, 2010). A smaller D value of 6–10 $\mu m^2\ s^{-1}$ is therefore expected for a protein with the mass of GFP–DapI (68 kDa), and of 4–6 $\mu m^2\ s^{-1}$ for the tetramer of GFP–DapI (272 kDa) observed by gel filtration (Fig. S1), as estimated from D for cytoplasmic GFP (27 kDa) assuming a simple $(mass)^{1/3}$ scaling of the hydrodynamic radius. According to these D values, in 30 ms monomeric and tetrameric GFP–DapI would move on average 0.8–1 μm and 0.7–0.8 μm respectively, making such foci irresolvable too. Thus, the fact that we could resolve clear foci of ~ 250 nm under 30 ms exposures suggests that GFP–DapI does not freely diffuse in the cytoplasm. Following the same equation, the diffusion coefficient for GFP–DapI foci travelling less than 250 nm over 30 ms would be $\leq 1\ \mu m^2\ s^{-1}$, which is at least ~ 10 times slower than a free diffusing GFP protein. This is surprisingly consistent with the diffusion coefficient reported for unpolymerized MreB ($1\ \mu m^2\ s^{-1}$) (Kim *et al.*,

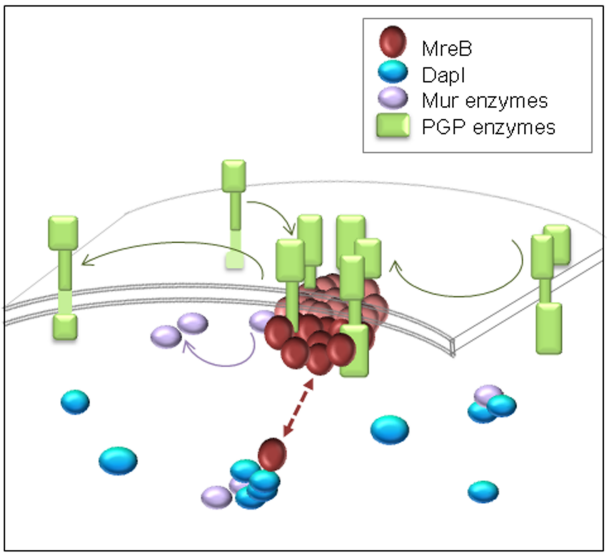

Fig. 7. Model for the co-ordination of intracellular and extracellular PG-synthesizing machineries by MreB. Most PG polymerizing (PGP) enzymes (in green) exhibit diffusing behaviour at the membrane (in grey); they do not move together with MreB (red) patches but are thought to dynamically associate with them, used as recruitment platforms that restrict their movement and orient their motion (Chastanet and Carballido-López, 2012). Some Mur enzymes (purple) were shown to display an MreB-like localization in *C. crescentus* (Divakaruni *et al.*, 2007; White *et al.*, 2010) and thus may interact with MreB patches at the membrane, ensuring efficient delivery of PG building blocks at the sites of their incorporation into the growing sacculus. DapI (blue), MurE and possibly other cytosolic PG precursor synthesizing enzymes of the DAP and the early Mur pathways, may interact in the cytoplasm with unpolymerized MreB, which is in equilibrium (red dashed line) with polymerized MreB at the membrane. If the physiologically interactive form of MreB with these PG precursor biosynthetic enzymes is unpolymerized, polymerization of MreB itself could contribute to the tight coupling required between the PG precursor- and the CW-synthesizing complexes.

2006). Thus, although slow diffusion of higher-order oligomeric forms of GFP–DapI impeded by crowding or meshwork in the cytoplasm cannot be excluded, it is tempting to speculate that DapI restricted diffusion in the cytoplasm may be mediated by its interaction with MreB.

The model in Fig. 7 illustrates where the MreB–DapI interaction may take place and highlights the plasticity and high dynamics of the individual CW biosynthetic complexes. Our findings provide an initial framework towards the understanding of the interactions between MreB proteins and the PG precursor biosynthetic machinery.

Experimental procedures

Complete details of all the materials and methods used are provided in the Supplemental Data.

Bacterial strains, plasmids and primers

Bacillus subtilis and *E. coli* strains and plasmids used in this study are listed in Supplementary Tables S1 and S2 respectively. The sequences of all oligonucleotide primers used in this study are listed in Table S3. The construction of strains is described in the Supplemental Data.

Yeast two-hybrid experiments

Genome-wide screens and specific two-hybrid experiments were performed as described previously (Carballido-López *et al*., 2006). A systematic verification of all interactions obtained in the screenings was performed experimentally as described in Marchadier *et al*. (2011).

Electron microscopy

For transmission electron microscopy (TEM), cells were harvested at the desired OD_{600} by gentle centrifugation, washed two times with PBS 1×, 2% glutaraldehyde and 0.1 M sodium cacodylate buffer pH 7.2, and kept 1–2 h at room temperature. Subsequent steps were performed mainly as described in Veiga *et al*. (2006). For scanning electron microscopy (SEM), exponentially growing cells were harvested by gentle centrifugation, resuspended in fixative solution (2.5% glutaraldehyde in 0.2 M sodium cacodylate buffer, pH 7.4) prior deposition on aluminium foil disc, and kept overnight at 4°C. Subsequent steps were performed mainly as described in Joly *et al*. (2010) except that following dehydration step, samples were subjected to critical-point drying under CO_2. TEM and SEM observations were done at the Microscopy and Imaging Platform MIMA2, INRA of Jouy-en-Josas and Massy respectively, France.

Analysis of cell wall thickness

Cell wall thickness was measured on TEM images of cross-sectioned cells using ImageJ (http://rsbweb.nih.gov/ij/). Several positions ($n \sim 15$–20) along a sidewall were measured per cell (no septal or polar regions were analysed). Cell wall thickness values were averaged and plotted as histograms using Sigmaplot (Systat software). All median and *P*-values (*t*-test) were similar whether we pooled all CW thickness values ($n > 130$) or used cellular averages ($n > 7$), indicating that thickness did not significantly vary among different cells of the same strain. The box plots shown in Fig. 3E were calculated from pooled thickness values. Box edges indicate 25th and 75th percentiles, line indicates median, whiskers indicate 10th and 90th percentiles and individual points indicate outliers. Distributions were compared using unpaired *t*-tests. Box plots and statistical analysis were performed with Matlab v. 7.5.0.338 (R2007b) Statistics Toolbox (v. 6.1) function ttest2.

Bright-field and epifluorescence microscopy

Epifluorescence microscopy was performed essentially as described previously (Carballido-López *et al*., 2006). FM4-64FX (Invitrogen) was used at 5 μg ml^{-1} for fluorescence staining of membranes. For vancomycin staining, fluorescently labelled vancomycin (Van-FL, Invitrogen) was mixed with an equal amount of unlabelled vancomycin (Van, Invitrogen) and added to growing cultures to a final concentration of 1 μg ml^{-1}. Cultures were incubated for 10 min at 30°C with agitation prior to observation.

Total internal reflection fluorescence (TIRF) and highly inclined and laminated optical sheet (HILO) microscopy

Cells from overnight cultures were diluted 1:1000 into fresh LB medium, allowed for further growth at 37°C to reach early exponential phrase, and immobilized on agarose pads. TIRFM and analysis of MreB patches dynamics were performed as described in Domínguez-Escobar *et al*. (2011). 100 ms exposure time and 2 s inter-frame were used in GFP–MreB time-lapses. TIRFM and HILO imaging of GFP and GFP–YkuR were done on an inverted microscope (Nikon Ti-E) with a diode-pumped solid-state laser (Cobolt Calypso, 50 mW, 491 nm) and an Apo TIRF 100× oil objective (Nikon, NA 1.49). All images were collected with an electron-multiplying charge-coupled device (EMCCD) camera (iXON3 DU-897, Andor) with a gain set at 300. Image acquisition was controlled by the software NIS-Elements. Time-lapse imaging was carried out under constant illumination with exposures of 10 ms or 30 ms and the highest frame rate possible (~ 14 or ~ 10 frames per second respectively). Incidence angles were adjusted manually for TIRF and HILO microscopy. Z-position was adjusted to obtain the best focus. All imaging processing was done in Matlab (Mathworks). For construction of Movie S1, a horizontal movie stack including three movies was generated in ImageJ. Individual image sequences were loaded into Matlab for batch processing and intensity scaled. The same greyscale was applied to the whole movie, where the pixels with the lowest, highest and other value in between were displayed as black (0), white (1) and intermediate shades of grey respectively. The resulting images were exported as a Quicktime movie in ImageJ (Movie S1).

Purification and analysis of cytoplasmic peptidoglycan precursors from B. subtilis

Briefly, *B. subtilis* cells were grown in LB supplemented with kanamycin to OD_{600} of 0.4–0.6. The pool of PG precursors was purified essentially as described previously (Ornelas-Soares *et al*., 1994) and subjected to reverse phase HPLC analysis on a Shimadzu HPLC system using a Hypersil ODS column in 100 mM $NaPO_4$ buffer at 52°C with a linear gradient from 5–24% methanol run over 80 min. Peaks of interest were collected manually, desalted and then analysed by mass spectrometry. Samples were spotted directly onto the MALDI plate using 5 mg ml^{-1} α-ciano-4-hydroxycinnaminic acid in 50% (v/v) acetonitrile, 5% (v/v) formic acid as the matrix. Mass spectra were acquired in reflectron positive and negative MS and MS/MS modes using a 4800 plus MALDI-TOF/TOF MS analyser (PO25MS). Mass spectrometry data were provided by the Mass Spectrometry Laboratory, Analytical Services Unit, Instituto de Tecnologia Química e Biológica, Universidade Nova de Lisboa, Portugal.

Acknowledgements

We are grateful to N. Campo for the anti-GFP antibody. We thank T. Meylheuc and S. Chat from the Microscopy and Imaging Platform MIMA2 (INRA, France), for SEM and TEM observations respectively. We thank the reviewers for their critical and constructive comments. MS data were provided by the INRA Platform for Proteomics Analysis of Paris South West (PAPPSO) and the Mass Spectrometry Laboratory, Analytical Services Unit, Instituto de Tecnologia Química e Biológica, Universidade Nova de Lisboa. Work in S.R.F. laboratory was funded by 'Fundação para a Ciência e Tecnologia' through research grant PTDC/BIA-MIC/100747/2008 and PEst-OE/EQB/LA0004/2011. Work in R.W.-S. and R.C.-L. laboratories was supported by young investigator grants from the Human Frontier Science Program Organization (HFSP-RGY0067/2009-C); the Max-Planck society (R.W.-S.) and the French National Research Agency (ANR-08-JCJC-0024-01 to R.C.-L.). A.C. was supported by a Marie Curie IRG (249018) and A.-S.R. by a PhD fellowship from the MICA department (INRA).

References

Anwar, R.A., and Vlaovic, M. (1986) UDP-N-acetylmuramoyl-L-alanyl-D-glutamyl-L-lysine synthetase from *Bacillus sphaericus*: activation by potassium phosphate. *Biochem Cell Biol* **64:** 297–303.

Auger, G., van Heijenoort, J., Vederas, J.C., and Blanot, D. (1996) Effect of analogues of diaminopimelic acid on the meso-diaminopimelate-adding enzyme from *Escherichia coli*. *FEBS Lett* **391:** 171–174.

Barreteau, H., Kovac, A., Boniface, A., Sova, M., Gobec, S., and Blanot, D. (2008) Cytoplasmic steps of peptidoglycan biosynthesis. *FEMS Microbiol Rev* **32:** 168–207.

Belitsky, B.R. (2002) Biosynthesis of amino acids of the glutamate and aspartate families, alanine, and polyamines. In Bacillus Subtilis *and Its Closest Relatives: From Genes to Cells*. Sonenshein, A.L., Hoch, A.A., and Losick, R. (eds). Washington, DC: ASM Press, pp. 203–231.

Bouhss, A., Trunkfield, A.E., Bugg, T.D., and Mengin-Lecreulx, D. (2008) The biosynthesis of peptidoglycan lipid-linked intermediates. *FEMS Microbiol Rev* **32:** 208–233.

Brans, A., Filee, P., Chevigne, A., Claessens, A., and Joris, B. (2004) New integrative method to generate *Bacillus subtilis* recombinant strains free of selection markers. *Appl Environ Microbiol* **70:** 7241–7250.

Carballido-López, R. (2006) The bacterial actin-like cytoskeleton. *Microbiol Mol Biol Rev* **70:** 888–909.

Carballido-López, R., Formstone, A., Li, Y., Ehrlich, S.D., Noirot, P., and Errington, J. (2006) Actin homolog MreBH governs cell morphogenesis by localization of the cell wall hydrolase LytE. *Dev Cell* **11:** 399–409.

Chastanet, A., and Carballido-López, R. (2012) The actin-like MreB proteins in *Bacillus subtilis*: a revolutionary dynamics. *Front Biosci (Schol Ed)* **4:** 1582–1606.

Chen, N.Y., Zhang, J.J., and Paulus, H. (1989) Chromosomal location of the *Bacillus subtilis* aspartokinase II gene and nucleotide sequence of the adjacent genes homologous to *uvrC* and *trx* of *Escherichia coli*. *J Gen Microbiol* **135:** 2931–2940.

Chen, N.Y., Jiang, S.Q., Klein, D.A., and Paulus, H. (1993) Organization and nucleotide sequence of the *Bacillus subtilis* diaminopimelate operon, a cluster of genes encoding the first three enzymes of diaminopimelate synthesis and dipicolinate synthase. *J Biol Chem* **268:** 9448–9465.

Cirilli, M., Zheng, R., Scapin, G., and Blanchard, J.S. (2003) The three-dimensional structures of the *Mycobacterium tuberculosis* dihydrodipicolinate reductase-NADH-2,6-PDC and -NADPH-2,6-PDC complexes. Structural and mutagenic analysis of relaxed nucleotide specificity. *Biochemistry* **42:** 10644–10650.

Daniel, R.A., and Errington, J. (2003) Control of cell morphogenesis in bacteria: two distinct ways to make a rod-shaped cell. *Cell* **113:** 767–776.

Dehmelt, L., and Bastiaens, P.I. (2010) Spatial organization of intracellular communication: insights from imaging. *Nat Rev Mol Cell Biol* **11:** 440–452.

Divakaruni, A.V., Baida, C., White, C.L., and Gober, J.W. (2007) The cell shape proteins MreB and MreC control cell morphogenesis by positioning cell wall synthetic complexes. *Mol Microbiol* **66:** 174–188.

Domínguez-Escobar, J., Chastanet, A., Crevenna, A.H., Fromion, V., Wedlich-Söldner, R., and Carballido-López, R. (2011) Processive movement of MreB-associated cell wall biosynthetic complexes in bacteria. *Science* **333:** 225–228 [Epub 2 Jun 2011].

Elowitz, M.B., Surette, M.G., Wolf, P.E., Stock, J.B., and Leibler, S. (1999) Protein mobility in the cytoplasm of *Escherichia coli*. *J Bacteriol* **181:** 197–203.

English, B.P., Hauryliuk, V., Sanamrad, A., Tankov, S., Dekker, N.H., and Elf, J. (2011) Single-molecule investigations of the stringent response machinery in living bacterial cells. *Proc Natl Acad Sci USA* **108:** E365–E373.

Favini-Stabile, S., Contreras-Martel, C., Thielens, N., and Dessen, A. (2013) MreB and MurG as scaffolds for the cytoplasmic steps of peptidoglycan biosynthesis. *Environ Microbiol* doi: 10.1111/1462-2920.12171 (in press).

Formstone, A., and Errington, J. (2005) A magnesium-dependent *mreB* null mutant: implications for the role of *mreB* in *Bacillus subtilis*. *Mol Microbiol* **55:** 1646–1657.

Gaballah, A., Kloeckner, A., Otten, C., Sahl, H.G., and Henrichfreise, B. (2011) Functional analysis of the cytoskeleton protein MreB from *Chlamydophila pneumoniae*. *PLoS ONE* **6:** e25129.

Gardete, S., Ludovice, A.M., Sobral, R.G., Filipe, S.R., de Lencastre, H., and Tomasz, A. (2004) Role of *murE* in the expression of beta-lactam antibiotic resistance in *Staphylococcus aureus*. *J Bacteriol* **186:** 1705–1713.

Garner, E.C., Bernard, R., Wang, W., Zhuang, X., Rudner, D.Z., and Mitchison, T. (2011) Coupled, circumferential motions of the cell wall synthesis machinery and MreB filaments in *B. subtilis*. *Science* **333:** 222–225.

Girish, T.S., Navratna, V., and Gopal, B. (2011) Structure and nucleotide specificity of *Staphylococcus aureus* dihydrodipicolinate reductase (DapB). *FEBS Lett* **585:** 2561–2567.

Grandgenett, D.P., and Stahly, D.P. (1971) Repression of diaminopimelate decarboxylase by L-lysine in different *Bacillus* species. *J Bacteriol* **105:** 1211–1212.

Graves, L.M., and Switzer, R.L. (1990) Aspartokinase III, a new isozyme in *Bacillus subtilis* 168. *J Bacteriol* **172:** 218–223.

Höltje, J.V. (1996) A hypothetical holoenzyme involved in the replication of the murein sacculus of *Escherichia coli*. *Microbiology* **142** (Part 8): 1911–1918.

Hutton, C.A., Southwood, T.J., and Turner, J.J. (2003) Inhibitors of lysine biosynthesis as antibacterial agents. *Mini Rev Med Chem* **3:** 115–127.

Ishihama, Y., Oda, Y., Tabata, T., Sato, T., Nagasu, T., Rappsilber, J., and Mann, M. (2005) Exponentially modified protein abundance index (emPAI) for estimation of absolute protein amount in proteomics by the number of sequenced peptides per protein. *Mol Cell Proteomics* **4:** 1265–1272.

Ito, E., and Strominger, J.L. (1973) Enzymatic synthesis of the peptide in bacterial uridine nucleotides. VII. Comparative biochemistry. *J Biol Chem* **248:** 3131–3136.

Jana, M., Luong, T.T., Komatsuzawa, H., Shigeta, M., and Lee, C.Y. (2000) A method for demonstrating gene essentiality in *Staphylococcus aureus*. *Plasmid* **44:** 100–104.

Janowski, R., Kefala, G., and Weiss, M.S. (2010) The structure of dihydrodipicolinate reductase (DapB) from *Mycobacterium tuberculosis* in three crystal forms. *Acta Crystallogr D Biol Crystallogr* **66:** 61–72.

Jenkins, A.H., Schyns, G., Potot, S., Sun, G., and Begley, T.P. (2007) A new thiamin salvage pathway. *Nat Chem Biol* **3:** 492–497.

Joly, F., Mayeur, C., Bruneau, A., Noordine, M.-L., Meylheuc, T., Langella, P., *et al*. (2010) Drastic changes in fecal and mucosa-associated microbiota in adult patients with short bowel syndrome. *Biochimie* **92:** 753–761.

Kawai, Y., Asai, K., and Errington, J. (2009a) Partial functional redundancy of MreB isoforms, MreB, Mbl and MreBH, in cell morphogenesis of *Bacillus subtilis*. *Mol Microbiol* **73:** 719–731.

Kawai, Y., Daniel, R.A., and Errington, J. (2009b) Regulation of cell wall morphogenesis in *Bacillus subtilis* by recruitment of PBP1 to the MreB helix. *Mol Microbiol* **71:** 1131–1144.

Kawai, Y., Marles-Wright, J., Cleverley, R.M., Emmins, R., Ishikawa, S., Kuwano, M., *et al*. (2011) A widespread family of bacterial cell wall assembly proteins. *EMBO J* **30:** 4931–4941.

Kim, S.Y., Gitai, Z., Kinkhabwala, A., Shapiro, L., and Moerner, W.E. (2006) Single molecules of the bacterial actin MreB undergo directed treadmilling motion in *Caulobacter crescentus*. *Proc Natl Acad Sci USA* **103:** 10929–10934.

Kobashi, N., Nishiyama, M., and Yamane, H. (2001) Characterization of aspartate kinase III of *Bacillus subtilis*. *Biosci Biotechnol Biochem* **65:** 1391–1394.

Kobayashi, K., Ehrlich, S.D., Albertini, A., Amati, G., Andersen, K.K., Arnaud, M., *et al*. (2003) Essential *Bacillus subtilis* genes. *Proc Natl Acad Sci USA* **100:** 4678–4683.

Kohlrausch, U., and Höltje, J.V. (1991) One-step purification procedure for UDP-N-acetylmuramyl-peptide murein precursors from *Bacillus cereus*. *FEMS Microbiol Lett* **62:** 253–257.

Kumar, M., Mommer, M.S., and Sourjik, V. (2010) Mobility of cytoplasmic, membrane, and DNA-binding proteins in *Escherichia coli*. *Biophys J* **98:** 552–559.

Lovering, A.L., Safadi, S.S., and Strynadka, N.C. (2012) Structural perspective of peptidoglycan biosynthesis and assembly. *Annu Rev Biochem* **81:** 451–478.

Marchadier, E., Carballido-López, R., Brinster, S., Fabret, C., Mervelet, P., Bessieres, P., *et al*. (2011) An expanded protein-protein interaction network in *Bacillus subtilis* reveals a group of hubs: exploration by an integrative approach. *Proteomics* **11:** 2981–2991.

Mengin-Lecreulx, D., Michaud, C., Richaud, C., Blanot, D., and van Heijenoort, J. (1988) Incorporation of LL-diaminopimelic acid into peptidoglycan of *Escherichia coli* mutants lacking diaminopimelate epimerase encoded by dapF. *J Bacteriol* **170:** 2031–2039.

Mengin-Lecreulx, D., Blanot, D., and van Heijenoort, J. (1994) Replacement of diaminopimelic acid by cystathionine or lanthionine in the peptidoglycan of *Escherichia coli*. *J Bacteriol* **176:** 4321–4327.

Michaud, C., Mengin-Lecreulx, D., van Heijenoort, J., and Blanot, D. (1990) Over-production, purification and properties of the uridine-diphosphate-N-acetylmuramoyl-L-alanyl-D-glutamate: meso-2,6-diaminopimelate ligase from *Escherichia coli*. *Eur J Biochem* **194:** 853–861.

Mohammadi, T., Karczmarek, A., Crouvoisier, M., Bouhss, A., Mengin-Lecreulx, D., and den Blaauwen, T. (2007) The essential peptidoglycan glycosyltransferase MurG forms a complex with proteins involved in lateral envelope growth as well as with proteins involved in cell division in *Escherichia coli*. *Mol Microbiol* **65:** 1106–1121.

Mohammadi, T., van Dam, V., Sijbrandi, R., Vernet, T., Zapun, A., Bouhss, A., *et al*. (2011) Identification of FtsW as a transporter of lipid-linked cell wall precursors across the membrane. *EMBO J* **30:** 1425–1432.

Munoz-Espin, D., Daniel, R., Kawai, Y., Carballido-López, R., Castilla-Llorente, V., Errington, J., *et al*. (2009) The actin-like MreB cytoskeleton organizes viral DNA replication in bacteria. *Proc Natl Acad Sci USA* **106:** 13347–13352.

Nenninger, A., Mastroianni, G., and Mullineaux, C.W. (2010) Size dependence of protein diffusion in the cytoplasm of *Escherichia coli*. *J Bacteriol* **192:** 4535–4540.

Nicolas, P., Mader, U., Dervyn, E., Rochat, T., Leduc, A., Pigeonneau, N., *et al*. (2012) Condition-dependent transcriptome reveals high-level regulatory architecture in *Bacillus subtilis*. *Science* **335:** 1103–1106.

Ornelas-Soares, A., de Lencastre, H., de Jonge, B.L., and Tomasz, A. (1994) Reduced methicillin resistance in a new *Staphylococcus aureus* transposon mutant that incorporates muramyl dipeptides into the cell wall peptidoglycan. *J Biol Chem* **269:** 27246–27250.

Osborn, M.J., and Rothfield, L. (2007) Cell shape determination in *Escherichia coli*. *Curr Opin Microbiol* **10:** 606–610.

Petricek, M., Rutberg, L., and Hederstedt, L. (1989) The structural gene for aspartokinase II in *Bacillus subtilis* is closely linked to the *sdh* operon. *FEMS Microbiol Lett* **52:** 85–87.

Richaud, C., Mengin-Lecreulx, D., Pochet, S., Johnson, E.J., Cohen, G.N., and Marliere, P. (1993) Directed evolution of biosynthetic pathways. Recruitment of cysteine thioethers for constructing the cell wall of *Escherichia coli*. *J Biol Chem* **268:** 26827–26835.

Rodionov, D.A., Vitreschak, A.G., Mironov, A.A., and Gelfand, M.S. (2003) Regulation of lysine biosynthesis and transport genes in bacteria: yet another RNA riboswitch? *Nucleic Acids Res* **31:** 6748–6757.

Rosner, A., and Paulus, H. (1971) Regulation of aspartokinase in *Bacillus subtilis*. The separation and properties of two isofunctional enzymes. *J Biol Chem* **246:** 2965–2971.

Roten, C.A., Brandt, C., and Karamata, D. (1991) Genes involved in meso-diaminopimelate synthesis in *Bacillus subtilis*: identification of the gene encoding aspartokinase I. *J Gen Microbiol* **137:** 951–962.

Scapin, G., Blanchard, J.S., and Sacchettini, J.C. (1995) Three-dimensional structure of *Escherichia coli* dihydrodipicolinate reductase. *Biochemistry* **34:** 3502–3512.

Scheffers, D.J., and Pinho, M.G. (2005) Bacterial cell wall synthesis: new insights from localization studies. *Microbiol Mol Biol Rev* **69:** 585–607.

Sobral, R.G., Ludovice, A.M., de Lencastre, H., and Tomasz, A. (2006) Role of *murF* in cell wall biosynthesis: isolation and characterization of a *murF* conditional mutant of *Staphylococcus aureus*. *J Bacteriol* **188:** 2543–2553.

Spira, F., Dominguez-Escobar, J., Muller, N., and Wedlich-Soldner, R. (2012) Visualization of cortex organization and dynamics in microorganisms, using total internal reflection fluorescence microscopy. *J Vis Exp* **63:** e3982.

van Teeffelen, S., Wang, S., Furchtgott, L., Huang, K.C., Wingreen, N.S., Shaevitz, J.W., and Gitai, Z. (2011) The bacterial actin MreB rotates, and rotation depends on cell-wall assembly. *Proc Natl Acad Sci USA* **108:** 15822–15827.

Tiyanont, K., Doan, T., Lazarus, M.B., Fang, X., Rudner, D.Z., and Walker, S. (2006) Imaging peptidoglycan biosynthesis in *Bacillus subtilis* with fluorescent antibiotics. *Proc Natl Acad Sci USA* **103:** 11033–11038.

Tokunaga, M., Imamoto, N., and Sakata-Sogawa, K. (2008) Highly inclined thin illumination enables clear single-molecule imaging in cells. *Nat Methods* **5:** 159–161.

Typas, A., Banzhaf, M., Gross, C.A., and Vollmer, W. (2012) From the regulation of peptidoglycan synthesis to bacterial growth and morphology. *Nat Rev Microbiol* **10:** 123–136.

Vagner, V., Dervyn, E., and Ehrlich, S.D. (1998) A vector for systematic gene inactivation in *Bacillus subtilis*. *Microbiology* **144** (Part 11): 3097–3104.

Veiga, P., Piquet, S., Maisons, A., Furlan, S., Courtin, P., Chapot-Chartier, M.-P., and Kulakauskas, S. (2006) Identification of an essential gene responsible for D-Asp incorporation in the *Lactococcus lactis* peptidoglycan crossbridge. *Mol Microbiol* **62:** 1713–1724.

Velasco, A.M., Leguina, J.I., and Lazcano, A. (2002) Molecular evolution of the lysine biosynthetic pathways. *J Mol Evol* **55:** 445–459.

Vollmer, W., and Bertsche, U. (2008) Murein (peptidoglycan) structure, architecture and biosynthesis in *Escherichia coli*. *Biochim Biophys Acta* **1778:** 1714–1734.

Weinberger, S., and Gilvarg, C. (1970) Bacterial distribution of the use of succinyl and acetyl blocking groups in diaminopimelic acid biosynthesis. *J Bacteriol* **101:** 323–324.

White, C.L., Kitich, A., and Gober, J.W. (2010) Positioning cell wall synthetic complexes by the bacterial morphogenetic proteins MreB and MreD. *Mol Microbiol* **76:** 616–633.

Zapun, A., Noirclerc-Savoye, M., Helassa, N., and Vernet, T. (2012) Peptidoglycan assembly machines: the biochemical evidence. *Microb Drug Resist* **18:** 256–260.

Zeghouf, M., Li, J., Butland, G., Borkowska, A., Canadien, V., Richards, D., *et al*. (2004) Sequential Peptide Affinity (SPA) system for the identification of mammalian and bacterial protein complexes. *J Proteome Res* **3:** 463–468.

Zhang, J.J., Hu, F.M., Chen, N.Y., and Paulus, H. (1990) Comparison of the three aspartokinase isozymes in *Bacillus subtilis* Marburg and 168. *J Bacteriol* **172:** 701–708.

Supporting information

Additional supporting information may be found in the online version of this article at the publisher's web-site.